 Extended Abstracts of the 2019 International Conference on Solid State Devices and Materials, Nagoya, 2019, pp1035-1036

Activation and Recrystallization of Ultra-High-Dose Phosphorus-Implanted Silicon using Multi-Pulse Nanosecond Laser Annealing

Hyunsu Shin[1], Hwa-yeon Ryu[1], Chang hun Song [1], Heungsoo Park[1], Dae-hong Ko[1*]

[1] Department of material science and engineering, Yonsei university, Korea
Phone: +81-2-2123-7739 E-mail: ulbba@yonsei.ac.kr

Abstract

Ultra-high-dose (2.5×10^{16} cm^{-2}) phosphorus-doped silicon is recrystallized during nanosecond laser annealing. After single-pulse laser annealing, end-of-range defects in the phosprous doped silison remains, but these defects are removed for the case of the ten-pulse annealed sample. The results show the recrystallization of a 3×10^{21} cm^{-3} phosphorus-doped silicon layer without defects after multi-pulse nanosecond laser annealing.

1. Introduction

In recent years, the semiconductor industry has been decreasing transistor sizes for reduced voltage and power consumption. As transistor size is scaled down, the effect of channel resistance on power consumption is minimized. However, the effect of contact resistance on the power consumption of metal-oxide-semiconductor field-effect transistors (MOSFETs) has increased since contact area decreases with transistor size being decreased. One way to keep low contact resistivity is to increase the active doping concentration of the source/drain. For N-type MOSFET, highly phosphorus doped silicon has been actively studied for achieving low contact resistivity [1-2].

The conventional method for phosphorus doping is ion implantation, but this can cause ion radiation damage (displacement of substrate atom from their lattice site) to the substrate [3]. Therefore, ion implantation must be accompanied by post-implant annealing in order to recover the damaged lattice. There are many studies on laser annealing to improve the quality of recrystallized layer [4].

In this presentation, we will show the behavior of the defects and the diffusion of phosphorus of the silicon samples before and after laser anneal. The electrical properties are also important for the source/drain. Thus, we measured electrical properties such as active sheet concentration using the Hall effect measurement method and achieved significant increase in phosphorus activation with laser annealing.

2. Experimental

A 6-inch, Czochralski-grown, p-type, 10-30 ohm·cm, (100) silicon wafer was used. Phosphorus was implanted at 25 keV with a total dose of 2.5×10^{16} cm^{-2} using a Varian high-current implanter, VIISTA80HP.

After the implantation, laser annealing was performed using a Coherent COMPEX205. The laser used KrF source gas of 248 nm wavelength and its pulse width was 24 nanoseconds. Samples were irradiated by single- and multi-pulse modes laser (repetition frequency of 1 Hz) with the energy densities of 450 and 600 mJ·cm^{-2}.

The microstructures of the as-implanted and laser-annealed samples were observed using high-resolution cross-sectional TEM with JEOL JEM-2100f. Samples were prepared with mechanical polishing and low-energy ion milling.

The dopant profile was analyzed using time-of-flight secondary ion mass spectrometry (TOF-SIMS) with IONTOF ToF-SIMS 5 system. Depth profile analysis was performed in dual-beam mode. Bi_1 with 30 keV accelerating voltage was used as the primary gun and Cesium ion with 1 keV accelerating voltage was secondary gun. The activated phosphorus concentration and electron mobility were determined through Hall effect measurements using the Ecopia HMS-5000 system at room temperature.

3. Result and Discussion

Fig. 1 shows the cross-sectional TEM images of the as-implanted and laser-annealed samples. As shown in Fig. 1(a), about 45 nm of the top layer was amorphized due to the ion radiation damage and underneath the amorphized layer, there are end of range (EOR) defects observed. Fig. 1(b) shows the TEM image of the 450 mJ·cm^{-2} single-pulse annealed sample; it clearly shows the recrystallization of the amorphized silicon layer of Fig. 1(a) and there are defects in the recrystallized layer extended from the interface between the amorphous silicon and single crystalline silicon. As shown in Fig. 1(c), the top layer of the 450 mJ·cm^{-2} 10 pulse annealed sample was recrystallized in the same way as that of the 450

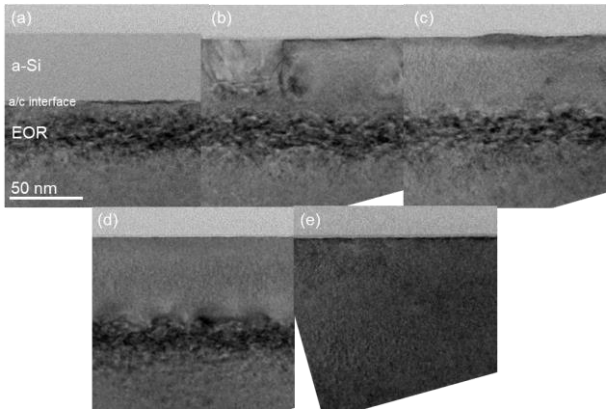

Fig. 1. Cross-sectional TEM micro graph of (a) as-implanted, after single-pulse laser anneaing with (b) 450 mJ·cm^{-2} (c) 600 mJ·cm^{-2}, and multi-pulse laser annealing with (d) 450 mJ·cm^{-2} (e) 600 mJ·cm^{-2}

mJ·cm^{-2} single-pulse annealed sample (Fig. 1(b)), but the

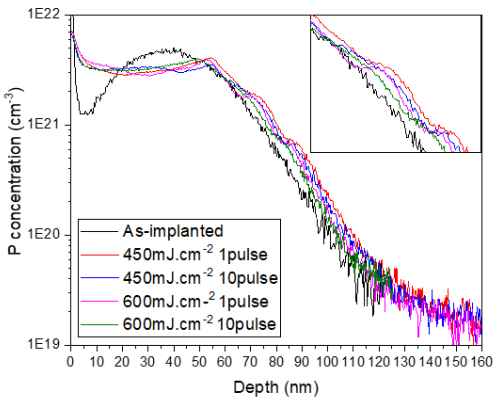

Fig. 3. Phosphorus SIMS profile of as-implanted laser annealed sample

number of defect for the 10 pulse annealed sample is much smaller than that for the single-pulse annealed sample. In Fig. 1(d), the number of defects in the 600 mJ·cm^{-2} single-pulse annealed sample is smaller than that in the 450 mJ·cm^{-2} single-pulse annealed sample (Fig. 1(b)).

There are some challenges over non-melt single crystalline silicon region; EOR defects are still remained after the laser anneal although the number of defects in the recrystallized layer is decreased. However, no observable defects are present in the EOR as well as the defects in recrystallized silicon for the case of the 600 mJ·cm^{-2} 10 pulse annealed sample (Fig. 1(e)).

Fig. 2 shows the phosphorus profiles of the samples before and after the laser annealing. The phosphorus concentration is 4.5 × 10^{21} cm^{-3} in the as-implanted sample. Unlike the as-implanted sample, a flat region is observed in the annealed samples. The thickness of the flat region is almost the same as the thickness of the amorphized layer in Fig. 1(a) (45 nm). Because the diffusivity of liquid silicon (~10^{-4} cm^2) is much higher than that of single crystalline silicon (10^{-12}-10^{-9} cm^2), phosphorus is distributed uniformly in melted silicon during laser annealing. At around 85 nm in depth, a kink is observed

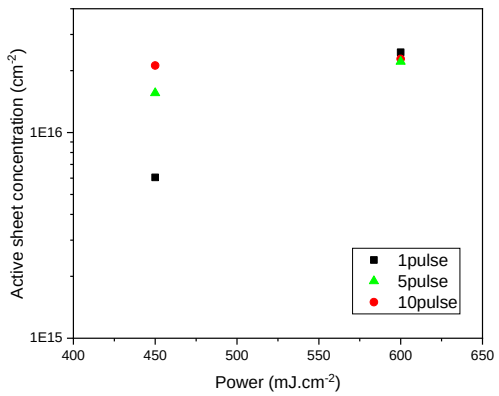

Fig. 2. Phosphorus SIMS profile of as-implanted laser annealed sample

in both the single-pulse annealed samples as well as in the 450 mJ·cm^{-2} 10 pulse annealed sample. This is due to the EOR defects in the annealed samples. The kink disappears in the 600 mJ·cm^{-2} 10 pulse annealed sample because the EOR defects were recovered, as shown in Fig. 1(e). Dopant diffusion is not observed in the flat region at all the annealing conditions.

The active sheet carrier concentration is an important property when considering applications of phosphorus-doped silicon to source/drains. Figure 3 shows the active sheet concentration of the laser annealed samples. For the 450 mJ·cm^{-2} single- pulse annealed sample, the active sheet concentration is 6.0 × 10^{15} cm^{-2}; it increases to 1.5 × 10^{16} and 2.1 × 10^{16} cm^{-2} for the 450 mJ·cm^{-2} five-pulse and ten-pulse annealed samples, respectively. For the 600 mJ·cm^{-2} single-pulse, five-pulse and ten-pulse samples, the active sheet concentration (2.5 × 10^{16} cm^{-2}) does not increase as the number of pulse increases because all the implanted phosphorus (2.5 × 10^{16} cm^{-2}) is already been activated during 600 mJ·cm^{-2} single-pulse annealing.

3. Conclusions

Nanosecond laser annealing was performed on phosphorus implanted silicon with single- and multi-pulse modes. The defects and electrical properties were characterized. Defect control is important in the application of phosphorus-doped silicon to source/drains because defects can degrade the electrical properties of transistors. The number of defects in the recrystallized layer as well as the number of EOR defects were decreased using multi-pulse laser annealing. Moreover, active phosphorus concentration is increased as laser power density and the number of laser pulse increases. So, we achieved 100% phosphorus activation without defects.

Acknowledgements

This work was supported by the Joint Program for Samsung Electronics-Yonsei University and the IT R&D program of MKE/KEIT (10067739, Development of Core Technologies for <5 nm Next-Generation Logic Devices).

References

[1] C. Ni, X. Li, S. Sharma, K. V Rao, M. Jin, C. Lazik, V. Banthia, B. Colombeau, N. Variam, A. Mayur, H. Chung, R. Hung, and A. Brand, 2015 Symp. VLSI Technol. **T118**, (2015).

[2] O. Gluschenkov, Z. Liu, H. Niimi, S. Mochizuki, J. Fronheiser, X. Miao, J. Li, J. Demarest, C. Zhang, C. Niu, B. Liu, A. Petrescu, P. Adusumilli, J. Yang, H. Jagannathan, H. Bu, and T. Yamashita, Tech. Dig. - Int. Electron Devices Meet. IEDM 17.2.1 (2017).

[3] J.F. Gibbons, Proc. IEEE **60**, 1062 (2008).

[4] J. Narayan, O.W. Holland, W.H. Christie, and J.J. Wortman, J. Appl. Phys. **57**, 2709 (1985).